Hindawi
Journal of Nanomaterials
Volume 2019, Article ID 3572317, 11 pages
https://doi.org/10.1155/2019/3572317

Review Article

Temperature-Dependent Morphology Evolution of Boron Nitride and Boron Carbonitride Nanostructures

Wei Li, Huan Yang, Shuaifeng Chen, Qing Chen, Lijie Luo, Jianbao Li, Yongjun Chen, and Changjiu Li

State Key Laboratory of Marine Resource Utilization in South China Sea, College of Materials and Chemical Engineering, Hainan University, Haikou 570228, China

Correspondence should be addressed to Yongjun Chen; chenyj99@163.com

Received 4 October 2018; Accepted 30 December 2018; Published 6 March 2019

Academic Editor: Giuseppe Compagnini

Copyright © 2019 Wei Li et al. This is an open access article distributed under the Creative Commons Attribution License, which permits unrestricted use, distribution, and reproduction in any medium, provided the original work is properly cited.

Boron nitride (BN) and boron carbonitride (BCN) nanostructures with versatile morphology were synthesized at different temperatures. The morphologies such as smooth microspheres, nanoflake-decorated microspheres, solid nanowires, hollow nanotubes (bamboo-like nanotubes, quasi-cylindrical nanotubes, and cylindrical nanotubes), and nanosheet-assembled microwires have been observed. Systematic investigation showed that the reaction temperature was responsible for the versatile morphologies through influencing the guiding effect of catalyst alloy droplet and the diffusion rates of growth species. The diffusion rate differences between surface diffusion (along the surface of the droplet) and bulk diffusion (through the bulk of the droplet) at different reaction temperatures were suggested to affect the final structure of the BN and BCN nanostructures.

1. Introduction

Boron nitride nanotubes (BNNTs) are structural analogues of carbon nanotubes (CNTs), alternating B and N atoms entirely substitute for C atoms in a graphitic-like sheet with almost no change in atomic spacing. BNNTs are considered to be a desirable candidate for potential applications in nanoelectronics [1], biomedical materials [2, 3], catalyst [4], and new composites [5, 6] because of their excellent resistance to oxidation (up to 900°C) [7], high chemical stability [8], high Young's modulus [9], and high thermal stability [10] and even the ability to suppress thermal neutron radiation [11]. In addition, BNNTs have a uniform wide bandgap of ~5.5 eV which is independent of tube chirality [12], while CNTs may be a metal or a narrow bandgap semiconductor, depending on the chirality and diameter. Ternary boron carbonitride nanotubes (BCNNTs), however, have tunable bandgaps determined merely by their chemical composition rather than geometrical structure, which is superior to the CNT and BNNT counterparts [13–15]. This gives BCNNTs potential applications in the fields of electrical conductors, electronic devices, photoluminescent materials, and catalysts [15–17].

It is well known that applications of BN and BCN are related to their purity, size, and morphology. To date, a series of methods have been successfully developed to prepare BN and BCN nanostructures such as arc discharge [18, 19], solid-state reaction [20–22], ball milling–annealing process [23, 24], chemical vapor deposition (CVD) method [25–29], and other methods. However, the morphologies of the synthesized BN and BCN nanostructures were versatile and could not be controlled currently. Thus, it is of great importance to investigate the dominant factors that affect the formation of BN and BCN nanostructures with versatile morphology. In fact, it has been noted that reaction temperature dramatically affected the formation and morphology of BN or BCN nanostructures [30–33]. In this work, the morphology evolutions of BN and BCN nanostructures and their relationship with reaction temperature have been studied systematically.

2. The Morphological Evolution of BN and BCN Nanostructures

Hollow BN microspheres were usually synthesized in our group by heating a paste-like mixture of amorphous B and Fe $(NO_3)_3{\cdot}9H_2O$ under flowing ammonia atmosphere at elevated temperatures [33]. The decomposition of Fe $(NO_3)_3$ produced Fe_2O_3, which reacted with B to generate B_2O_2 vapor and Fe catalyst, and further reaction between B_2O_2 and NH_3 assisted by the catalyst resulted in the formation of BN products (Figure 1). It can be seen that smooth BN microspheres were prepared at a lower temperature of 1100°C (Figure 1(a)), while rough BN microspheres decorated with thin nanoflakes on their surfaces were obtained at 1200°C and 1300°C (Figures 1(b) and 1(c)). The inset transmission electron microscopy (TEM) image revealed the hollow nature of the microspheres. High-resolution TEM (HRTEM) characterization and energy-dispersive X-ray spectrometer (EDX) result demonstrated the BN composition of both the microspheres and nanoflakes. The diameters of microspheres and the thicknesses of nanoflakes were 0.8–3 μm and 2–7 nm, respectively. The vapor-liquid-solid (VLS) mechanism was responsible for the formation of the BN microspheres. The VLS model was firstly put forward by Warner in the synthesis of silicon fibre and can be described as two parts [34]. First, the reaction raw material is vaporized into atomic vapor (B_2O_2) at a high temperature and collides with gas molecules (NH_3), rapidly cooling into a supercooled gas and forming a low-combination catalyst droplet in a lower temperature region. An interface between the gas phase and the substrate is formed, where the reaction molecules in the gas phase are continuously adsorbed. After reaching supersaturation, crystal nuclei are deposited, and with further absorption of B and N species, smooth BN hollow microspheres are finally formed. The main involved reactions as follows were proposed, and thermodynamics calculation revealed the feasibility (equations 1-3).

$$2Fe(OH)_3(s) \rightarrow Fe_2O_3(s) + 3H_2O(g) \quad \Delta G_{1100\text{-}1300^\circ C} = -434.1 \sim -503.5\,\text{kJ} \tag{1}$$

$$6B(s) + 2Fe_2O_3(s) \rightarrow 3B_2O_2(g) + 4Fe(l) \quad \Delta G_{1100\text{-}1300^\circ C} = -540.8 \sim -652.5\,\text{kJ} \tag{2}$$

$$B_2O_2(g) + 2NH_3(g) \rightarrow 2BN(s) + 2H_2O(g) + H_2(g) \quad \Delta G_{1100\text{-}1300^\circ C} = -322.3 \sim -307.4\,\text{kJ} \tag{3}$$

Bae et al. [35] also found that reaction temperature had a great influence on the morphology of one-dimensional (1D) BN nanostructures when heating the precursors of ball-milled boron and $FeCl_2{\cdot}4H_2O$. Exclusively, bamboo-like BN nanotubes with thick compartments were formed when the temperature was 1050°C, while cylindrical BN nanotubes with thin even no compartments were synthesized when the temperature increased to 1200°C, as have been illustrated in Figure 2.

A similar phenomenon was also observed in our group when a novel chemical vapor deposition method was employed to synthesize 1D BN nanostructures directly on stainless-steel foils [25, 36]. In this method, boron and zinc oxide (ZnO) powders were annealed under a nitrogen-containing atmosphere (e.g., N_2 together with H_2). The medium product B_2O_2 vapor was generated by the reaction between B and ZnO, which then reacted with N_2 and H_2 and produced BN. The stainless-steel foils not only served as the substrate but also provided Fe-containing catalyst due to their partial melting at experimental temperatures. It was found that solid BN nanowires were formed at 1100°C (Figure 3(a)) [36], and hollow bamboo-like BN nanotubes were fabricated when the reaction temperature increased to 1200°C (Figure 3(b)) [25]. Interestingly, a combined BN nanostructure composed of hollow bamboo-like nanotube and solid nanowire was also found (Figure 3(c)). The thermodynamics calculation indicates that the following reactions could occur (equations 4-6):

$$2B(s) + 2ZnO(s) \rightarrow 2Zn(g) + B_2O_2(g) \quad \Delta G_{1050\text{-}1200^\circ C} = -92.4 \sim -156.6\,\text{kJ} \tag{4}$$

$$B_2O_2(g) + N_2(g) + 2H_2(g) \rightarrow 2BN(s) + 2H_2O(g) \quad \Delta G_{1050\text{-}1200^\circ C} = -127.2 \sim -80.7\,\text{kJ} \tag{5}$$

$$2B(s) + 2ZnO(s) + N_2(g) + 2H_2(g) \rightarrow 2BN(s) + 2H_2O(g) + 2Zn(g) \quad \Delta G_{1050\text{-}1200^\circ C} = -219.6 \sim -237.3\,\text{kJ} \tag{6}$$

Temperature effect on the morphology of 1D BN nanostructures was further confirmed by us when a coprecipitation and annealing route was employed to synthesize BN nanotubes using raw materials of amorphous boron, iron nitrate nonahydrate (Fe $(NO_3)_3{\cdot}9H_2O$), and urea (CO $(NH_2)_2$) [37]. The hydroxyl groups generated from the excess hydrolysis of urea restrained the reaction between H_2O and Fe $(OH)_3$ (that was produced by the reaction of urea with Fe $(NO_3)_3$), lowering the loss of Fe catalyst during the process of washing.

Only BN particles could be obtained when the annealing temperature was 1100°C (Figure 4(a)), but both bamboo-like and quasi-cylindrical BN nanotubes were prepared at 1200°C (Figure 4(b)). When the annealing temperature further increased to 1300°C, however, a micro-nano composite structure (we called it nanoflake-decorated nanotube) was fabricated (Figure 4(c)). TEM characterization clearly showed that bamboo-like and quasi-cylindrical BN nanotubes were prepared at 1200°C (Figures 4(d)-4(f)) and nanoflake-decorated BN nanotubes formed at 1300°C (Figure 4(g)). HRTEM characterization (Figure 4(h)) further confirmed the BN composition and crystalline nature of the nanotubes and nanoflakes. We believed that the very fast nitridation reaction of boron at a higher temperature (e.g., 1300°C) could generate excess BN species, which deposited on the surface of the already grown bamboo-like nanotubes

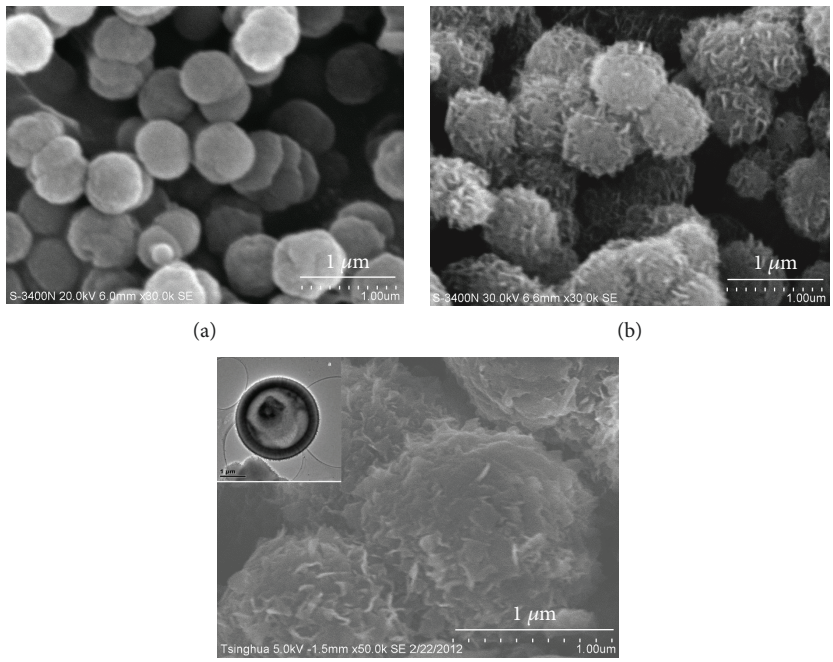

(a) (b)

(c)

Figure 1: SEM images of BN microspheres synthesized at different temperatures. (a) Smooth microspheres fabricated at 1100°C. Nanoflake-decorated microspheres obtained at (b) 1200°C and (c) 1300°C. The inset TEM image showed the hollow nature of a microsphere [33].

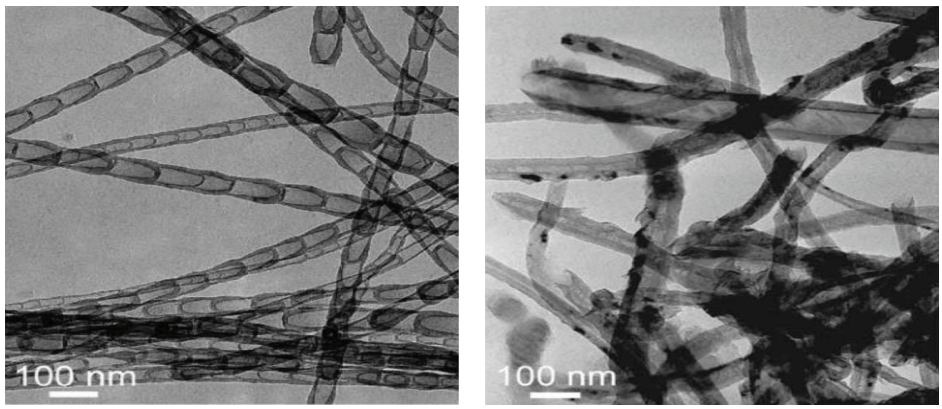

(a) (b)

Figure 2: TEM images of BN nanostructures. (a) Bamboo-like nanotubes formed at 1050°C and (b) cylindrical nanotubes grown at 1200°C [35].

in the form of nanoflakes [37, 38]. The main reactions were suggested (equations 7-12).

$$3CO(NH_2)_2(s) + 9H_2O(l) + 2Fe(NO_3)_3(s) \rightarrow 6NH_4NO_3(l) + 3CO_2(g) + 2Fe(OH)_3(s) \quad (7)$$

$$Fe(OH)_3(s) + 6H_2O(l) \rightarrow \left[Fe(H_2O)_6\right]^{3+}(l) + 3OH^-(l) \quad (8)$$

$$2Fe(OH)_3(s) \rightarrow Fe_2O_3(s) + 3H_2O(g)$$
$$\Delta G_{1100\text{-}1300\circ C} = -434.1 \sim -503.5\,\text{kJ} \quad (9)$$

$$Fe_2O_3(s) + 4B(s) \rightarrow 2FeB(s) + B_2O_3(s)$$
$$\Delta G_{1100\text{-}1300\circ C} = -612.1 \sim -617.4\,\text{kJ} \quad (10)$$

$$2FeB(s) + 2NH_3(g) \rightarrow 2BN(s) + 2Fe(s) + 3H_2(g)$$
$$\Delta G_{1100\text{-}1300\circ C} = -330.6 \sim -345.2\,\text{kJ} \quad (11)$$

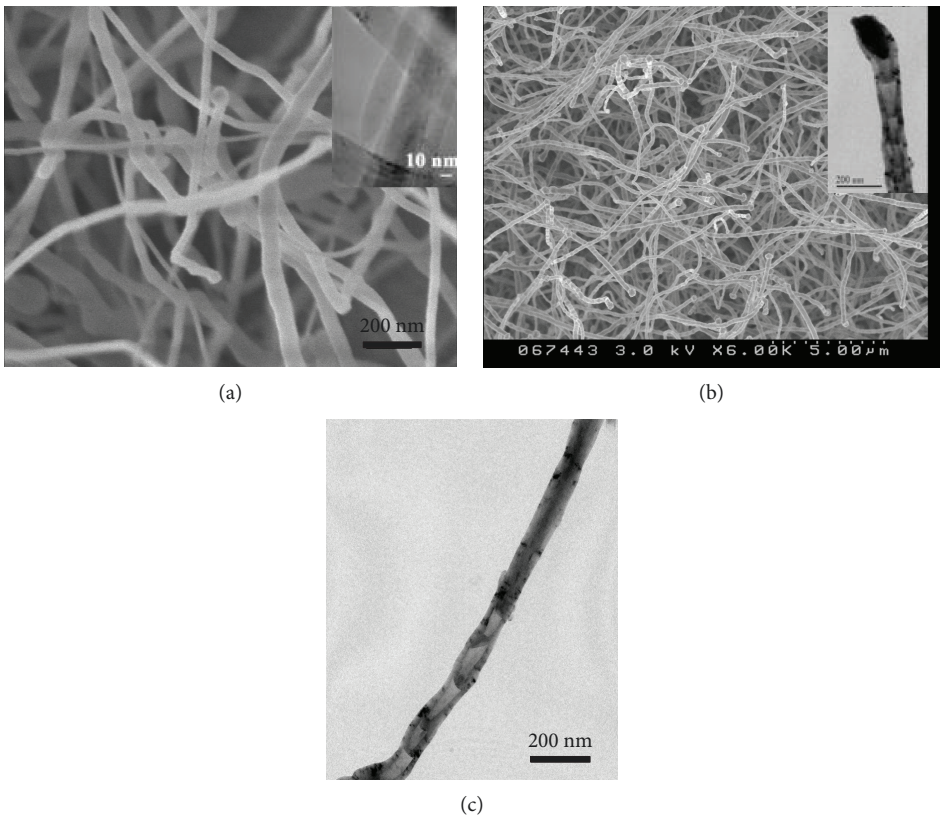

(a) (b)

(c)

Figure 3: BN nanostructures synthesized directly on stainless-steel foils at different temperatures. (a) SEM image of solid BN nanowires prepared at 1100°C and the corresponding TEM image (inset). (b) SEM image of bamboo-like BN nanotubes prepared at 1200°C and the TEM image (inset). (c) A combined BN nanostructure consisted of solid nanowire and bamboo-like nanotube [25, 36].

$$B_2O_3(s) + 2NH_3(g) \rightarrow 2BN(s) + 3H_2O(g)$$
$$\Delta G_{1100\text{-}1300^{\circ}C} = -46.0 \sim -65.7\,\text{kJ} \quad (12)$$

To widen the application area of BN nanotubes, it is of great significance to explore efficient routes for synthesizing BN nanotubes in large quantity and with high purity. A solid-state reaction method was developed in our group by annealing amorphous boron and ferric chloride ($FeCl_3{\cdot}6H_2O$) in flowing ammonia [20], realizing the goal of high purity and large quantity. In this process, the vital species BCl_3 vapor was generated through the reaction between B and $FeCl_2$ (derived from the reduction of $FeCl_3$ with NH_3), which further reacted with NH_3 to produce BN product with the assistance of Fe catalyst.

When the temperature was 1150°C, BN particles were mainly formed (Figure 5(a)). If the temperature increased to 1200°C and 1250°C, high-purity bamboo-like nanotubes and quasi-cylindrical nanotubes were prepared (Figures 5(b) and 5(c)), respectively. Besides, nanosheet-assembled microwires could be found in the up-layer of the product (Figure 5(d)) [39]. TEM characterization (the inset) verified that the microwire has a bamboo-like nanotube core. The enlarged SEM image clearly showed that the nanosheets are mostly separated with bending and crumpling morphology and nearly vertically aligned to the trunk (Figure 5(e)). Meanwhile, the nanosheet-assembled microwires have a distinct thickening in diameter with increasing temperature (Figure 5(f)). The following reactions were suggested (equations 13-16):

$$6FeCl_3(s) + 2NH_3(g) \rightarrow 6FeCl_2(s) + 6HCl(g) + N_2(g)$$
$$\Delta G_{25\text{-}1200\circ C} = -357.0 \sim -937.2\,\text{kJ} \quad (13)$$

$$FeCl_2(s) \rightarrow FeCl_2(l) \quad \Delta G_{1150\text{-}1250\circ C} = -14.8 \sim -24.6\,\text{kJ} \quad (14)$$

$$FeCl_2(l) + 2B(s) \rightarrow 2BCl_3(g) + 3Fe(l)$$
$$\Delta G_{1150\text{-}1250\circ C} = -88.7 \sim -97.0\,\text{kJ} \quad (15)$$

$$BCl_3(g) + NH_3(g) \rightarrow BN(s) + 3HCl(g)$$
$$\Delta G_{1150\text{-}1250\circ C} = -216.0 \sim -226.0\,\text{kJ} \quad (16)$$

Therefore, it can be seen that the morphology of BN products with increasing temperature could be transformed from the microsphere (or particle) to the solid nanowire, bamboo-like nanotube, quasi-cylindrical nanotube, cylindrical nanotube, and finally nanosheet- (nanoflake-) assembled microwires. Interestingly, a similar morphology evolution with increasing temperature was also observed in ternary BCN 1D nanostructures. A solid-state reaction route to the

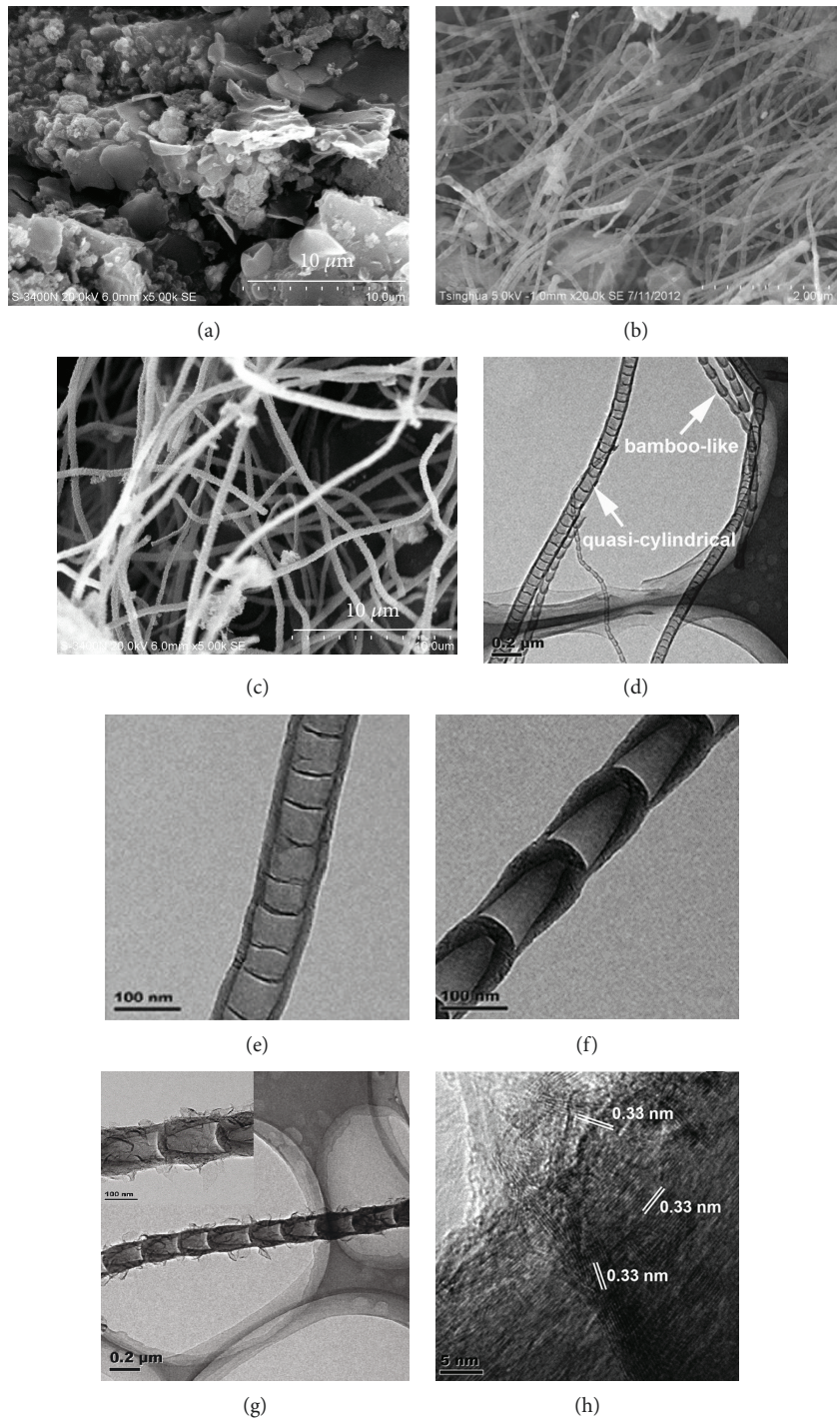

Figure 4: SEM images of BN product fabricated by heating raw material system of amorphous boron, iron nitrate nonahydrate ($Fe(NO_3)_3{\cdot}9H_2O$) and urea ($CO(NH_2)_2$) at different temperatures. (a) Irregular particles at 1100°C. (b) Bamboo-like nanotubes at 1200°C. (c) Nanoflake-decorated BN nanotubes at 1300°C. (d)-(f) TEM images revealed the coexistence of bamboo-like and quasi-cylindrical nanotubes. (g) A low magnification TEM image of a nanoflake-decorated nanotube. The inset shows the high magnification TEM image. (h) A high-resolution TEM image of a part of nanoflake-decorated nanotube [37].

synthesis of BCN nanotubes in large quantity was demonstrated in our group, by heating ball-milled mixture powders of amorphous boron and activated charcoal with a small amount of iron oxide (Fe_2O_3) under a mixture gas flow of $N_2 + H_2$ [22]. The catalyst of Fe was generated through the reduction of Fe_2O_3 with H_2. Bamboo-like BCN nanotubes were mainly formed when the reaction temperature was 1000°C (Figure 6(a)), and both bamboo-like and quasi-cylindrical BCN nanotubes coexisted when the temperature rose to 1100°C (Figures 6(b)–6(d)), while cylindrical BCN nanotubes were synthesized if the temperature further increased to 1200°C (Figure 6(e)).

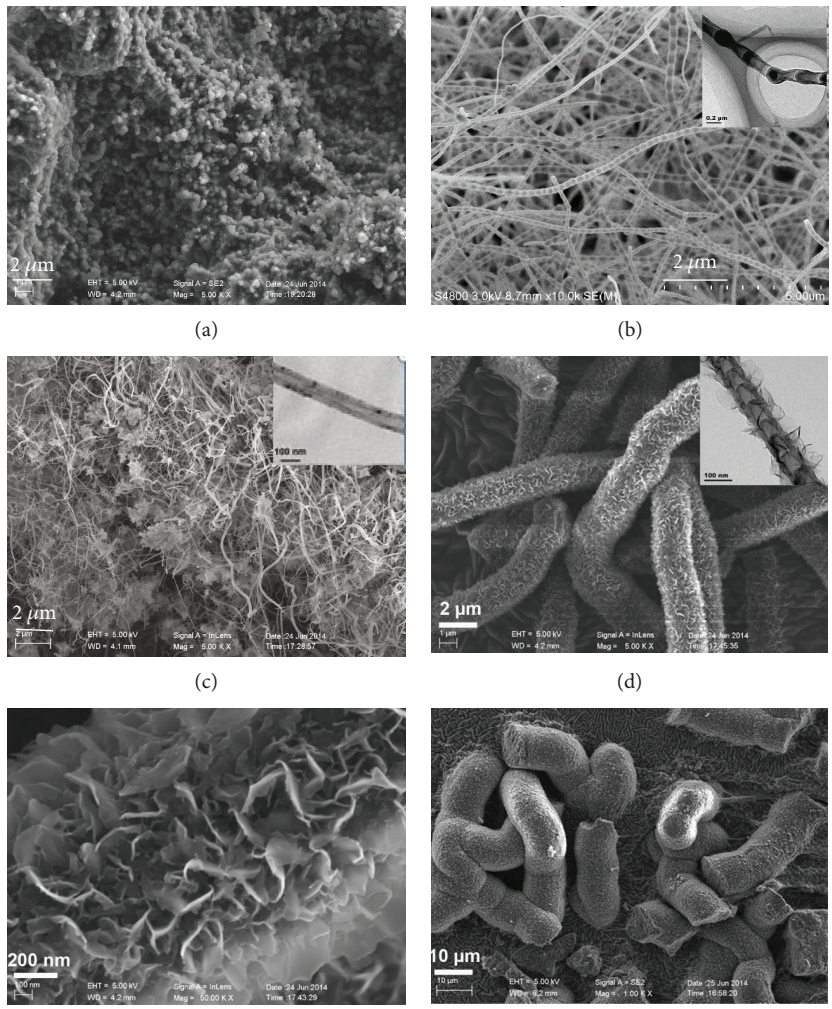

Figure 5: SEM images of BN products synthesized by heating boron powder and ferric chloride at different temperatures. (a) Particles obtained at 1150°C. (b) Bamboo-like nanotubes prepared at 1200°C. The inset is a TEM image. (c) Quasi-cylindrical nanotubes at 1250°C. The inset is a TEM image. (d) Thin nanosheet-assembled microwires prepared at 1200°C. The inset TEM image depicts the assembly of nanosheets from a bamboo-like nanotube core. (e) An enlarged SEM image, revealing the numerous thin nanosheets clearly. (f) Thick nanosheet-assembled microwires grown at 1250°C [20].

3. Morphology Evolution Mechanism

Based on the experimental results described above, we propose the morphology evolution model shown in Figure 7, and here, BN is discussed as a representative. It was believed that in the case of VLS growth of 1D nanostructures, one of the most important roles of catalyst alloy droplets was to provide critical nucleation sites [40]. The catalyst alloy droplets (e.g., Fe-Cr-Ni, FeB, and Fe) usually come from the substrate (e.g., stainless steel foil) or from the precursor of catalyst (e.g., Fe_2O_3, $FeCl_3$, and Fe $(NO_3)_3$). Apparently, the state and size of catalyst particles, which strongly depended on the reaction temperature, are the preconditions that determine the nucleation behavior and postnucleation growth of the BN nanostructures. For example, it has been reported that increasing temperature could result in the coarsening of alloy droplets, and larger FeB alloy droplets (larger than 200 nm) favored the formation of BN microspheres, while smaller ones (less than 100 nm) were conducive to the growth of 1D BN nanostructures [41, 42]. In addition, the catalyst particle in a liquid or quasi-liquid state is favorable for the nucleation and growth of BN crystals via the VLS process. If the reaction temperature is not high enough, catalyst particles may be still in a solid state, the VLS mechanism does not work, and the product often consists of irregular particles.

Figure 7 shows the morphology evolution of BN nanostructures with increasing reaction temperature. Particularly, (A) to (E) illustrates the BN microspheres originating from a larger catalyst alloy droplet. Liquid or quasi-liquid catalyst alloy droplet is generated at high temperature (e.g., 1100°C) first. Boron-containing vapor (e.g., B_2O_2) and nitrogen-containing gas (NH_3 or N_2) are absorbed and dissolved into the droplet, which produces BN species through their reaction (Figure 7(A)) [33, 43]. When the concentration of BN species in the droplet is greater than the saturation threshold, BN crystal begins to precipitate and BN

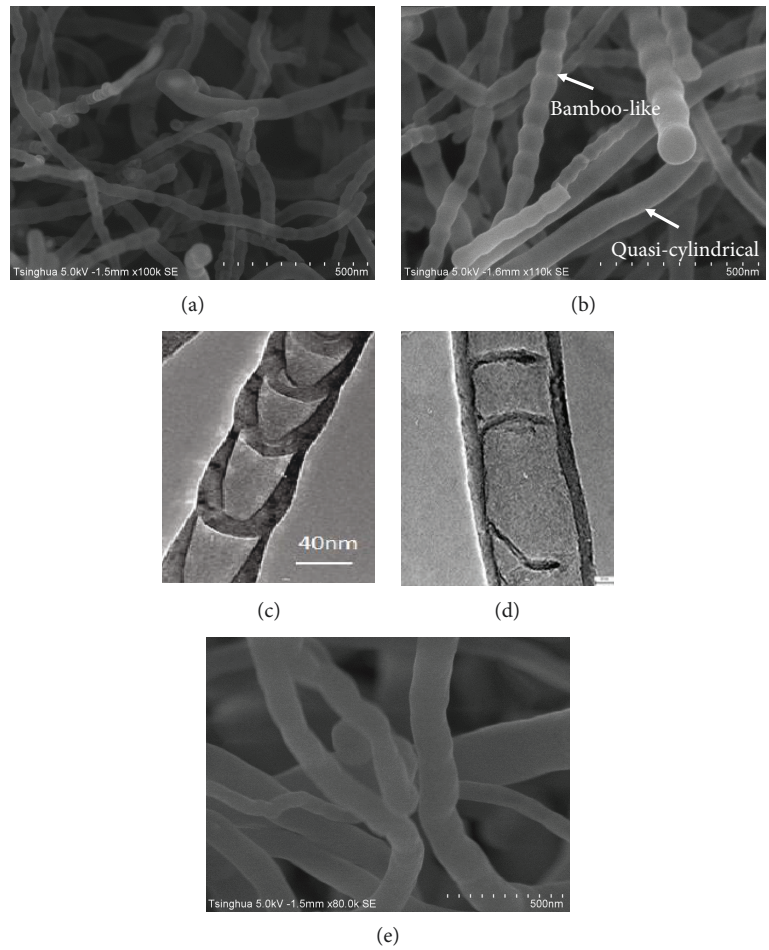

Figure 6: SEM images of the BCN nanotubes prepared at different temperatures. (a) Bamboo-like nanotubes synthesized at 1000°C. (b) Bamboo-like and quasi-cylindrical nanotubes coexisted at 1100°C. TEM characterization shows the (c) bamboo-like and (d) quasi-cylindrical nanotubes. (e) Cylindrical nanotubes formed at 1200°C [22].

shell is formed around the outline of the droplet (Figure 7(B)). With the continuous dissolution and reaction of boron-containing vapor and nitrogen-containing gas, BN shells will be thickened and lifted. As a result, a core–shell structure is formed around the droplet due to the lack of capillary effects (Figure 7(C)) [44]. Meanwhile, strain energy is generated between the BN shell and catalyst alloy droplet (core). When the thickness of shell reaches to a critical value, the exceeded strain energy will push the catalyst droplet core out via a dewetting process by the driving force of the Kirkendall effect [44–46]. Consequently, smooth BN hollow microsphere is formed (Figure 7(D)). When the reaction temperature increases (e.g., 1200°C and 1300°C), excess BN species (in addition to the consumption for the formation of BN microsphere) will be generated because of the fast reaction among the raw materials, which causes the direct deposition of these surplus BN species on the shell via a vapor-solid (VS) process which was proposed by Frank [47] in the growth mechanism research of Sn whiskers based on dislocation theory. At the crystal growth temperature, the active gas is adsorbed onto the surface of the spiral dislocation steps located in crystal growth interface, forming a crystal nucleus. When the nucleus reaches the critical value, it grows along the direction of the dislocated Bergs vector under the stress of the curvature. Therefore, nanoflakes are formed on the surface of the already grown microsphere, and finally, a nanoflake-decorated BN microsphere is formed (Figure 7(E)). Particularly, the defects on the surface of the microsphere are also favorable for the deposition of BN species and the resultant formation of BN nanoflakes.

However, if the catalyst alloy droplets are small enough, 1D BN nanostructures instead of microspheres are usually obtained. Moreover, the temperature-dependent morphological evolution of 1D nanostructures is totally different from that of the microspheres because of the capillary effect and guiding effect of the catalyst droplets. At a lower temperature, boron-containing vapor and nitrogen-containing gas are absorbed, dissolved, and reacted in the droplet, followed by the precipitation of BN crystal from the droplet when the concentration of BN species is greater than the saturation threshold (Figure 7(F)). With the continuous supply of B and N source, BN species will diffuse through both the surface and bulk of the droplet, and the catalyst alloy droplet will be lifted up by BN crystal (Figure 7(G)). When the temperature rises, both the surface diffusion rate (υ_s) and the bulk diffusion rate (υ_b) of BN species increase, but υ_s

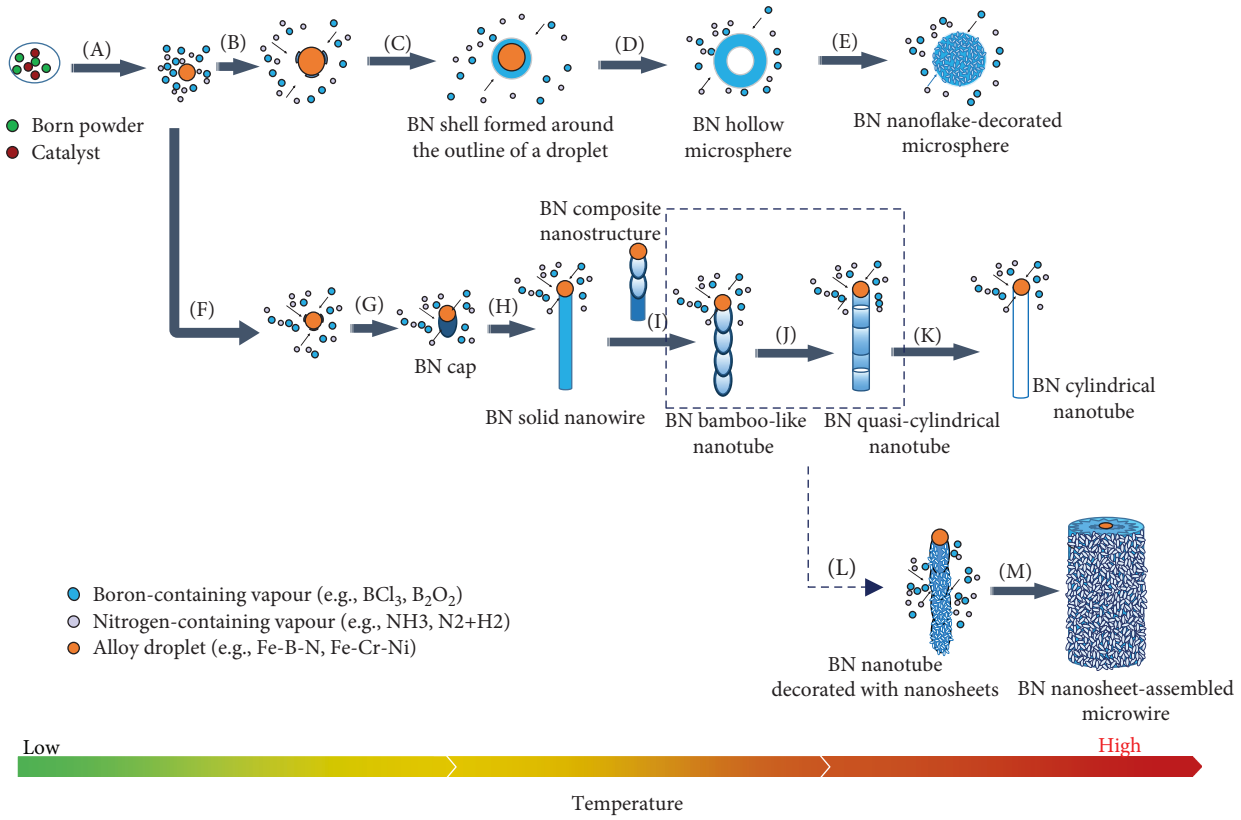

Figure 7: Morphology evolution of BN nanostructures with increasing reaction temperature.

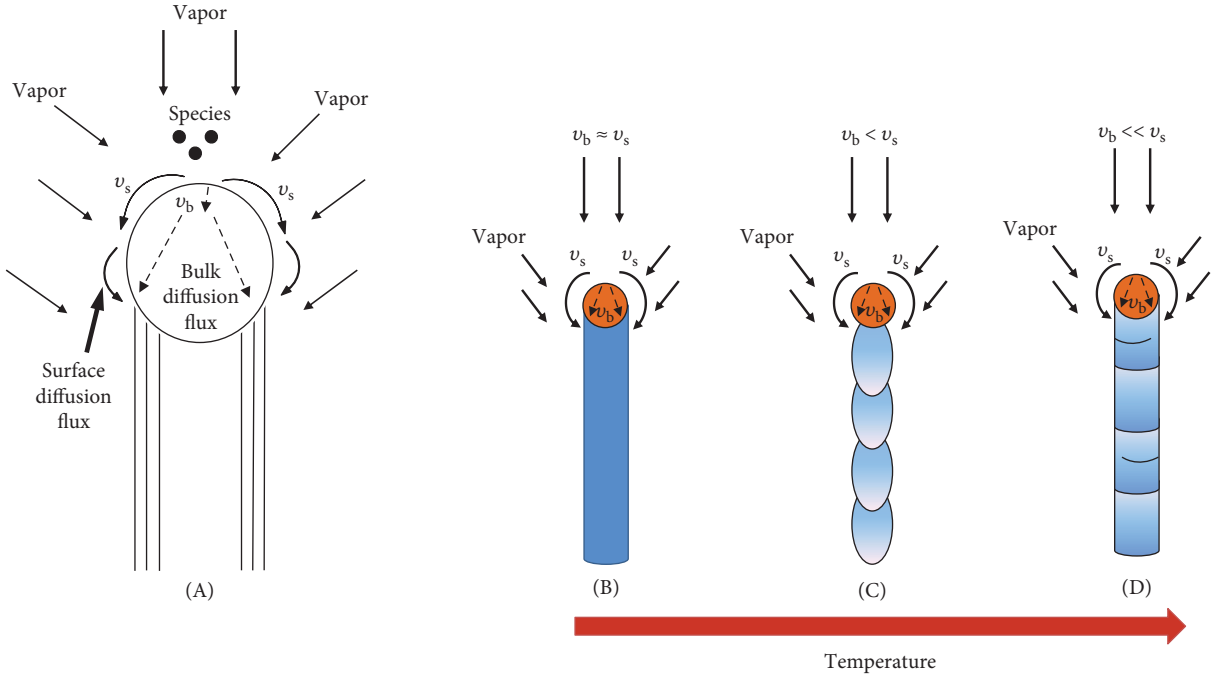

Figure 8: Sketch growth model of BN one-dimensional nanostructure. (A) BN pathways feeding BN growth via (i) impingement of BN flux into the BN surface and surface diffusion over crystal to the BN edge and (ii) direct impingement of B/N into the catalyst alloy droplet and bulk diffusion through the droplet to the BN edge. (B-D) Growth process varied with increasing temperature. (υ_s: surface diffusion rate, υ_b: bulk diffusion rate).

increases faster than υ_b. And the difference between υ_s and υ_b will be more and more significant with the further increase of temperature, which causes the morphological evolution of 1D nanostructure from solid nanowire (Figure 7(H)) to bamboo-like nanotube (Figure 7(I)), quasi-cylindrical nanotube (Figure 7(J)), and finally cylindrical nanotube (Figure 7(K)).

Figure 8 depicts the temperature effect on the diffusion rate of BN species and the resultant morphology evolution of BN 1D nanostructure. Usually, the growth of 1D BN nanostructure is determined simultaneously by (i) impingement of BN flux into the BN crystal surface and the surface diffusion over crystal to the BN edge and (ii) direct impingement of BN flux into the catalyst alloy droplet and the bulk diffusion through the droplet to the BN edge (Figure 8(A))[48]. At a given impingement flux of BN, the diffusion rate is the key factor that affects the morphology of BN crystal [49, 50]. At a lower temperature, the difference between υ_s and υ_b is small, and thereby BN crystal will grow homogeneously which leads to the formation of solid BN nanowire (Figure 8(B)). As reaction temperature rises, υ_s increases faster than υ_b [51], causing a rapid longitudinal growth of the BN cap from the droplet. In this circumstance, tensional force is produced at the interface between the BN cap and the droplet. The droplet is finally lifted up by the stress under the curvature, thus hollow BN cap is formed [44, 52–54]. The continuous diffusion of BN species along the droplet surface makes BN multisheets grow layer by layer along the (002) plane and nanotube wall will form [21, 48, 55, 56]. When the nanotube wall grows, BN species also precipitate inside the droplet via bulk diffusion, resulting in the formation of BN compartment layer. The compartment layer will connect with the wall and grow together for a while, and eventually depart from the droplet due to the stress accumulated under the curved compartment layers. As the joint of the compartment and the wall occurs in cycles, the bamboo-like nanotube is finally formed (Figure 8(C)) [25, 28]. However, the diffusion rate difference between υ_s and υ_b becomes more and more significant when the temperature further rises [51], which will favor the formation of nanotube walls rather than the compartment layers [35, 57]. Therefore, a quasi-cylindrical nanotube with thin compartments will be formed (Figure 8(D)). And if the temperature is high enough, υ_s is far larger than υ_b, causing the formation of the cylindrical nanotube. Moreover, the crystalline perfection of the nanotube also improves with increasing temperature, and the thin compartment layers will bear stronger and stronger stress. According to the principle of minimum free energy, cylindrical nanotube without compartment layers prefers to be formed [21, 35, 37].

In addition, it was reported that bamboo-like BN nanotubes had rough surfaces, and there were many defects existing on the surfaces, which could serve as new nucleation sites for the further growth of BN crystal [33, 39, 58, 59]. Excess BN species resulted from the fast nitridation of boron at high temperature would directly deposit on these nucleation sites. Moreover, BN species are reported to have sufficiently high mobility. Thus, BN species quickly diffuse on the surface and deposit on the defects, forming the primary nanosheets. The incoming BN species continuously land on the surface of the growing nanosheets and rapidly move along the surface toward the edge of the nanosheets and covalently bond to the edge atoms before being reevaporated, while those BN species diffusing toward the nanotube instead of the growing edges can be reevaporated due to the weak van der Waals forces attaching them to the nanotubes. So, the nanosheets tend to grow higher rather than thicker. With the accumulation of sustaining BN species, the nanosheets keep growing radially while the bottom part becomes compact on account of the branching and thickening of the nanosheets. In this process, VS mechanism governs the formation of BN nanosheets. Therefore, a nanosheet-assembled microwire is obtained (Figures 7(L) and 7(M)). It should be noted here that when raw materials of boron powder and ferric chloride were employed to synthesize BN nanostructures (as is discussed and shown in Figure 5), BN bamboo-like nanotubes and BN nanosheet-assembled microwires are formed in the lower and upper layer of the product, respectively. It is believed that BN species generated by the reaction between NH_3 and BCl_3 vapor have different concentrations in different layers of the powder bed [38]. The concentration of BN species in the upper layer is higher than that of BN species in the lower layer because of the blocking effect of the powder bed, which results in the formation of nanosheet-assembled microwires in the upper layer and bamboo-like nanotubes in the lower layer, respectively.

4. Conclusions

In summary, reaction temperature plays a dominant role in the morphological and structural evolution of the BN and BCN nanostructures. When the reaction temperature is lower, liquid or quasi-liquid catalyst droplets are hardly formed and irregular particle product is usually obtained. When the temperature increases, liquid or quasi-liquid catalyst droplets are formed which exhibits the guiding effect and capillary effect on the growth of products. Larger liquid droplets usually lead to the formation of microspheres, while smaller liquid droplets favor the generation of 1D nanostructures. In this case, the surface diffusion rate (υ_s) of growth species gradually exceeds the bulk diffusion rate ($\upsilon_{b)}$ with increasing temperature, which leads to the morphological evolution of 1D nanostructures from solid nanowire to bamboo-like nanotube, quasi-cylindrical nanotube, and finally cylindrical nanotube. The improvement of crystalline perfection of the nanotubes with increasing temperature also favors the final formation of cylindrical nanotubes without compartment layers inside the nanotubes. The defects, usually existing on the rough surface of BN microspheres and bamboo-like nanotubes, could serve as new nucleation sites for the excess BN species, resulting in the formation of BN nanoflake-decorated microspheres or nanosheet-assembled microwires.

Conflicts of Interest

The authors declare no conflict of interest.

Acknowledgments

This work is supported by the Natural Science Foundation of Hainan Province (No. 518MS021), the National Natural Science Foundation of China (No. 51702072, 51362008), and the Graduate Student Innovation Project of Hainan Province (No. Hyb2017-01).

References

[1] G. Li, Y. Zhao, J. Li et al., "Synthesis, characterization, physical properties, and OLED application of single BN-fused perylene diimide," *Journal of Organic Chemistry*, vol. 80, no. 1, pp. 196–203, 2014.

[2] M. A. Fernandez-Yague, A. Larrañaga, O. Gladkovskaya et al., "Effects of polydopamine functionalization on boron nitride nanotube dispersion and cytocompatibility," *Bioconjugate Chemistry*, vol. 26, no. 10, pp. 2025–2037, 2015.

[3] X. Li, X. Wang, X. Jiang et al., "Boron nitride nanotube-enhanced osteogenic differentiation of mesenchymal stem cells," *Journal of Biomedical Materials Research Part B: Applied Biomaterials*, vol. 104, no. 2, pp. 323–329, 2016.

[4] N. Meyer, C. Renders, R. Lanckman, M. Devillers, and S. Hermans, "Gold as active phase of BN-supported catalysts for lactose oxidation," *Applied Catalysis A: General*, vol. 504, pp. 549–558, 2015.

[5] L. Li, Y. Chen, and Z. H. Stachurski, "Boron nitride nanotube reinforced polyurethane composites," *Progress in Natural Science: Materials International*, vol. 23, no. 2, pp. 170–173, 2013.

[6] R. Agrawal, A. Nieto, H. Chen, M. Mora, and A. Agarwal, "Nanoscale damping characteristics of boron nitride nanotubes and carbon nanotubes reinforced polymer composites," *ACS Applied Materials & Interfaces*, vol. 5, no. 22, pp. 12052–12057, 2013.

[7] Y. Chen, J. Zou, S. J. Campbell, and G. Le Caer, "Boron nitride nanotubes: pronounced resistance to oxidation," *Applied Physics Letters*, vol. 84, no. 13, pp. 2430–2432, 2004.

[8] D. Golberg, Y. Bando, K. Kurashima, and T. Sato, "Synthesis and characterization of ropes made of BN multiwalled nanotubes," *Scripta Materialia*, vol. 44, no. 8-9, pp. 1561–1565, 2001.

[9] R. Arenal, M. S. Wang, Z. Xu, A. Loiseau, and D. Golberg, "Young modulus, mechanical and electrical properties of isolated individual and bundled single-walled boron nitride nanotubes," *Nanotechnology*, vol. 22, no. 26, article 265704, 2011.

[10] N. Kostoglou, K. Polychronopoulou, and C. Rebholz, "Thermal and chemical stability of hexagonal boron nitride (h-BN) nanoplatelets," *Vacuum*, vol. 112, pp. 42–45, 2015.

[11] M. L. Cohen and A. Zettl, "The physics of boron nitride nanotubes," *Physics Today*, vol. 63, no. 11, pp. 34–38, 2010.

[12] X. Blase, A. Rubio, S. G. Louie, and M. L. Cohen, "Stability and band gap constancy of boron nitride nanotubes," *Europhysics Letters (EPL)*, vol. 28, no. 5, pp. 335–340, 1994.

[13] M. Kawaguchi, "B/C/N materials based on the graphite network," *Advanced Materials*, vol. 9, no. 8, pp. 615–625, 1997.

[14] X. Blase, J.-C. Charlier, A. De Vita, and R. Car, "Theory of composite $B_xC_yN_z$ nanotube heterojunctions," *Applied Physics Letters*, vol. 70, no. 2, pp. 197–199, 1997.

[15] S. Azevedo, A. Rosas, M. Machado, J. R. Kaschny, and H. Chacham, "Effects of deformation on the electronic properties of B–C–N nanotubes," *Journal of Solid State Chemistry*, vol. 197, pp. 254–260, 2013.

[16] S. Wang, E. Iyyamperumal, A. Roy, Y. Xue, D. Yu, and L. Dai, "Vertically aligned BCN nanotubes as efficient metal-free electrocatalysts for the oxygen reduction reaction: a synergetic effect by co-doping with boron and nitrogen," *Angewandte Chemie International Edition*, vol. 50, no. 49, pp. 11756–11760, 2011.

[17] D. Golberg, P. S. Dorozhkin, Y. Bando et al., "Structure, transport and field-emission properties of compound nanotubes: CN_x vs. BNC_x (x <0.1)," *Applied Physics A: Materials Science & Processing*, vol. 76, no. 4, pp. 499–507, 2003.

[18] A. Loiseau, F. Willaime, N. Demoncy et al., "Boron nitride nanotubes," *Carbon*, vol. 36, no. 5-6, pp. 743–752, 1998.

[19] O. Stephan, P. M. Ajayan, C. Colliex et al., "Doping graphitic and carbon nanotube structures with boron and nitrogen," *Science*, vol. 266, no. 5191, pp. 1683–1685, 1994.

[20] A. Pan and Y. Chen, "Large-scale fabrication of boron nitride nanotubes with high purity via solid-state reaction method," *Nanoscale Research Letters*, vol. 9, no. 1, p. 555, 2014.

[21] Y. Chen, L. T. Chadderton, J. F. Gerald, and J. S. Williams, "A solid-state process for formation of boron nitride nanotubes," *Applied Physics Letters*, vol. 74, no. 20, pp. 2960–2962, 1999.

[22] L. Mo, Y. Chen, and L. Luo, "Solid-state reaction synthesis of boron carbonitride nanotubes," *Applied Physics A*, vol. 100, no. 1, pp. 129–134, 2010.

[23] J. Kim, S. Lee, Y. R. Uhm, J. Jun, C. K. Rhee, and G. M. Kim, "Synthesis and growth of boron nitride nanotubes by a ball milling–annealing process," *Acta Materialia*, vol. 59, no. 7, pp. 2807–2813, 2011.

[24] G. Wen, T. Zhang, X. X. Huang, B. Zhong, X. D. Zhang, and H. M. Yu, "Synthesis of bulk quantity BN nanotubes with uniform morphology," *Scripta Materialia*, vol. 62, no. 1, pp. 25–28, 2010.

[25] Y. Chen, L. Luo, L. Zhou, L. Mo, and Z. Tong, "Facile synthesis of boron nitride nanotubes and improved electrical conductivity," *Journal of Nanoscience and Nanotechnology*, vol. 10, no. 2, pp. 871–876, 2010.

[26] L. Luo, L. Mo, Z. Tong, and Y. Chen, "Facile synthesis of ternary boron carbonitride nanotubes," *Nanoscale Research Letters*, vol. 4, no. 8, pp. 834–838, 2009.

[27] G. Zhang, Z. Liu, L. Zhang, L. Jing, and K. Shi, "Growth and characterization of BCN nanotubes with high boron and nitrogen content," *Journal of Chemical Sciences*, vol. 125, no. 5, pp. 1169–1176, 2013.

[28] J. Li, J. Li, Y. Yin, Y. Chen, and X. Bi, "Water-assisted chemical vapor deposition synthesis of boron nitride nanotubes and their photoluminescence property," *Nanotechnology*, vol. 24, no. 36, article 365605, 2013.

[29] D. Özmen, N. A. Sezgi, and S. Balcı, "Synthesis of boron nitride nanotubes from ammonia and a powder mixture of boron and iron oxide," *Chemical Engineering Journal*, vol. 219, no. 3, pp. 28–36, 2013.

[30] P. Ahmad, M. U. Khandaker, Z. R. Khan, and Y. M. Amin, "Synthesis of boron nitride nanotubes via chemical vapour deposition: a comprehensive review," *RSC Advances*, vol. 5, no. 44, pp. 35116–35137, 2015.

[31] M. Bechelany, A. Brioude, S. Bernard, P. Stadelmann, D. Cornu, and P. Miele, "Boron nitride multiwall nanotubes

decorated with BN nanosheets," *CrystEngComm*, vol. 13, no. 21, 2011.

[32] J. Yu, J. Ahn, S. F. Yoon et al., "Semiconducting boron carbonitride nanostructures: nanotubes and nanofibers," *Applied Physics Letters*, vol. 77, no. 13, pp. 1949–1951, 2000.

[33] J. Li, H. Lin, Y. Chen, Q. Su, and X. Bi, "Synthesis and anti-oxidation performance of nanoflake-decorated boron nitride hollow microspheres," *Journal of Alloys and Compounds*, vol. 550, pp. 292–296, 2013.

[34] R. L. Barns and W. C. Ellis, "Whisker crystals of gallium arsenide and gallium phosphide grown by the vapor-liquid-solid mechanism," *Journal of Applied Physics*, vol. 36, no. 7, pp. 2296–2301, 1965.

[35] S. Y. Bae, H. W. Seo, J. Park, Y. S. Choi, J. C. Park, and S. Y. Lee, "Boron nitride nanotubes synthesized in the temperature range 1000–1200 °C," *Chemical Physics Letters*, vol. 374, no. 5-6, pp. 534–541, 2003.

[36] Y. J. Chen, B. Chi, D. C. Mahon, and Y. Chen, "An effective approach to grow boron nitride nanowires directly on stainless-steel substrates," *Nanotechnology*, vol. 17, no. 12, pp. 2942–2946, 2006.

[37] X. Bi, Y. Yin, J. Li, Y. Chen, J. Li, and Q. Su, "A co-precipitation and annealing route to the large-quantity synthesis of boron nitride nanotubes," *Solid State Sciences*, vol. 25, pp. 39–44, 2013.

[38] H. Yu, X. Huang, G. Wen, T. Zhang, B. Zhong, and H. Bai, "A facile method for synthesis of novel coral-like boron nitride nanostructures," *Materials Chemistry and Physics*, vol. 129, no. 1-2, pp. 30–34, 2011.

[39] A. Pan, Y. Chen, and J. Li, "An effective route for the synthesis of boron nitride micro-nano structures and the growth mechanism," *CrystEngComm*, vol. 17, no. 5, pp. 1098–1105, 2015.

[40] J. Li, H. Lin, Y. Chen, Q. Su, and Q. Huang, "The effect of iron oxide on the formation of boron nitride nanotubes," *Chemical Engineering Journal*, vol. 174, no. 2-3, pp. 687–692, 2011.

[41] A. Gorbunov, O. Jost, W. Pompe, and A. Graff, "Role of the catalyst particle size in the synthesis of single-wall carbon nanotubes," *Applied Surface Science*, vol. 197-198, pp. 563–567, 2002.

[42] K. P. Loh, M. Lin, M. Yeadon, C. Boothroyd, and Z. Hu, "Growth of boron nitride nanotubes and iron nanowires from the liquid flow of FeB nanoparticles," *Chemical Physics Letters*, vol. 387, no. 1-3, pp. 40–46, 2004.

[43] S. Trasobares, O. Stéphan, C. Colliex, W. K. Hsu, H. W. Kroto, and D. R. M. Walton, "Compartmentalized CN_x nanotubes: chemistry, morphology, and growth," *Journal of Chemical Physics*, vol. 116, no. 20, pp. 8966–8972, 2002.

[44] M. Yeadon, M. Lin, K. P. Loh, C. B. Boothroyd, J. Fu, and Z. Hu, "Direct observation of boron nitride nanocage growth by molecular beam nitridation and liquid-like motion of Fe–B nanoparticles," *Journal of Materials Chemistry*, vol. 13, no. 10, pp. 2573–2576, 2003.

[45] H. J. Fan, M. Knez, R. Scholz et al., "Influence of surface diffusion on the formation of hollow nanostructures induced by the Kirkendall effect: the basic concept," *Nano Letters*, vol. 7, no. 4, pp. 993–997, 2007.

[46] H. J. Fan, U. Gösele, and M. Zacharias, "Formation of nanotubes and hollow nanoparticles based on Kirkendall and diffusion processes: a review," *Small*, vol. 3, no. 10, pp. 1660–1671, 2007.

[47] F. C. Frank, "XC. On tin whiskers," *The London, Edinburgh, and Dublin Philosophical Magazine and Journal of Science*, vol. 44, no. 355, pp. 854–860, 2010.

[48] O. A. Louchev, T. Laude, Y. Sato, and H. Kanda, "Diffusion--controlled kinetics of carbon nanotube forest growth by chemical vapor deposition," *Journal of Chemical Physics*, vol. 118, no. 16, pp. 7622–7634, 2003.

[49] O. A. Louchev, "Surface diffusion growth and stability mechanism of BN nanotubes produced by laser beam heating under superhigh pressures," *Applied Physics Letters*, vol. 71, no. 24, pp. 3522–3524, 1997.

[50] L. T. Chadderton and Y. Chen, "Nanotube growth by surface diffusion," *Physics Letters A*, vol. 263, no. 4-6, pp. 401–405, 1999.

[51] O. A. Louchev, "Transport-kinetical phenomena in nanotube growth," *Journal of Crystal Growth*, vol. 237-239, pp. 65–69, 2002.

[52] X. X. Zhang, Z. Q. Li, G. H. Wen, K. K. Fung, J. Chen, and Y. Li, "Microstructure and growth of bamboo-shaped carbon nanotubes," *Chemical Physics Letters*, vol. 333, no. 6, pp. 509–514, 2001.

[53] R. T. K. Baker, M. A. Barber, P. S. Harris, F. S. Feates, and R. J. Waite, "Nucleation and growth of carbon deposits from the nickel catalyzed decomposition of acetylene," *Journal of Catalysis*, vol. 26, no. 1, pp. 51–62, 1972.

[54] L. T. Chadderton and Y. Chen, "A model for the growth of bamboo and skeletal nanotubes: catalytic capillarity," *Journal of Crystal Growth*, vol. 240, no. 1-2, pp. 164–169, 2002.

[55] S. K. Singhal, A. K. Srivastava, and R. B. Mathur, "Growth of boron nitride nanotubes having large surface area using mechanothermal process," *World Journal of Nano Science and Engineering*, vol. 1, no. 4, pp. 119–128, 2011.

[56] Y. Chen, M. J. Conway, J. D. Fitz Gerald, J. S. Williams, and L. T. Chadderton, "The nucleation and growth of carbon nanotubes in a mechano-thermal process," *Carbon*, vol. 42, no. 8-9, pp. 1543–1548, 2004.

[57] N. S. Kim, Y. T. Lee, J. Park et al., "Dependence of the vertically aligned growth of carbon nanotubes on the catalysts," *Journal of Physical Chemistry B*, vol. 106, no. 36, pp. 9286–9290, 2002.

[58] E. Bengu and L. D. Marks, "Single-walled BN nanostructures," *Physical Review Letters*, vol. 86, no. 11, pp. 2385–2387, 2001.

[59] J. J. Velázquez-Salazar, E. Muñoz-Sandoval, J. M. Romo-Herrera et al., "Synthesis and state of art characterization of BN bamboo-like nanotubes: evidence of a root growth mechanism catalyzed by Fe," *Chemical Physics Letters*, vol. 416, no. 4-6, pp. 342–348, 2005.


The Scientific
World Journal
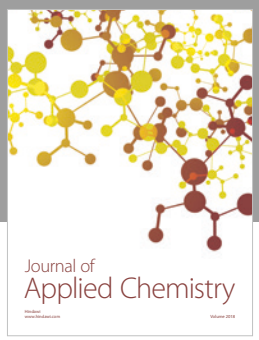
Journal of
Applied Chemistry
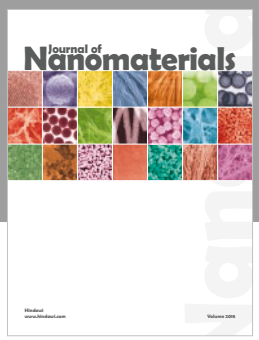
Journal of
Nanomaterials

Scientifica

International Journal of
Polymer Science
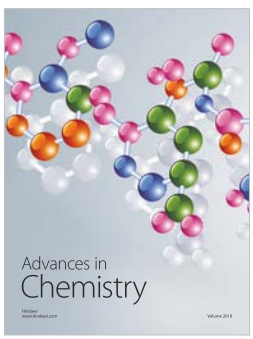
Advances in
Chemistry

Hindawi
Submit your manuscripts at
www.hindawi.com
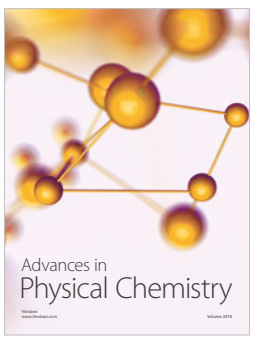
Advances in
Physical Chemistry

International Journal of
Analytical Chemistry
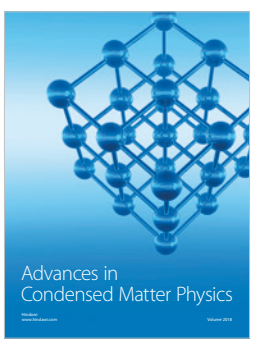
Advances in
Condensed Matter Physics
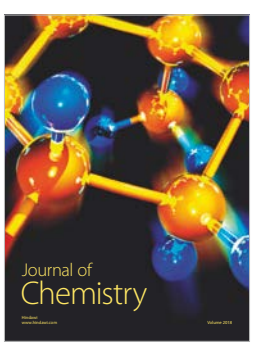
Journal of
Chemistry

International Journal of
Biomaterials
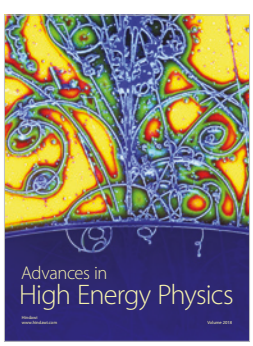
Advances in
High Energy Physics

Journal of
Engineering

Journal of
Nanotechnology

International Journal of
Corrosion

Journal of
Materials

BioMed
Research International
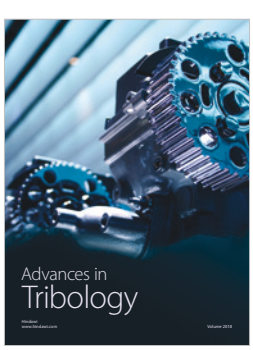
Advances in
Tribology
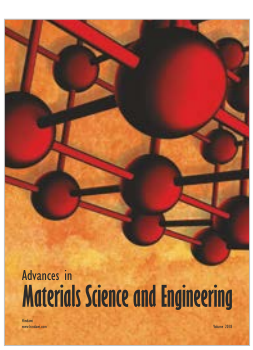
Advances in
Materials Science and Engineering